

pubs.acs.org/JACS Communication

Enzyme Responsive Rigid-Rod Aromatics Target "Undruggable" Phosphatases to Kill Cancer Cells in a Mimetic Bone Microenvironment

Meihui Yi, Fengbin Wang, Weiyi Tan, Jer-Tsong Hsieh,* Edward H. Egelman,* and Bing Xu*



Cite This: J. Am. Chem. Soc. 2022, 144, 13055-13059



ACCESS I

III Metrics & More

Article Recommendations

Supporting Information

ABSTRACT: Bone metastasis remains a challenge in cancer treatment. Here we show enzymatic responsive rigid-rod aromatics acting as the substrates of "undruggable" phosphatases to kill cancer cells in a mimetic bone microenvironment. By phosphorylation and conjugating nitrobenzoxadiazole (NBD) to hydroxybiphenylcarboxylate (BP), we obtained pBP-NBD (1P) as a substrate of both acid and alkaline phosphatases. 1P effectively kills both metastatic castration-resistant prostate cancer cells (mCRPCs) and osteoblast mimic cells in their coculture. 1P enters Saos2 almost instantly to target the endoplasmic reticulum (ER) of the cells. Coculturing with Saos2 cells boosts the cellular uptake of 1P by mCRPCs. Cryo-EM reveals the nanotube structures of both 1P (2.4 Å resolution, pH 5.6) and 1 (2.2 Å resolution, pH 7.4). The helical packing of both nanotubes is identical, held together by strong pistacking interactions. Besides reporting the atomistic structure of nanotubes formed by the assembly of rigid-rod aromatics, this work expands the pool of molecules for designing EISA substrates that selectively target TME.

his communication reports the first example of enzymeinstructed self-assembly (EISA) of rigid-rod aromatics for killing cancer cells in a mimetic bone microenvironment. Despite considerable progress in cancer therapy, tumor metastasis still causes most of cancer-related deaths.1 For example, approximately 90% of patients who die of prostate cancer have bone metastases.2 Bone metastases are a vicious selfreinforcing cycle in tumor microenvironments (TMEs), where cancer cells promote the differentiation of osteoclasts and osteoblasts, and the increased bone turnover releases cytokines to benefit metastatic cancer cells. Moreover, bone is also a site for further spread of other metastasis.3 The current treatment of bone metastasis, Radium-223 (Ra-223),4,5 is only palliative because the acceptable radiation dosage of Radium-223 is limited. Thus, there is an urgent need to develop novel approaches for killing cancer cells in bone metastasis sites or TME with minimal side effects. Inspired by the dual targeting mode-of-action of Radium-223, we are aiming to develop nonradioactive small molecules as a single agent that selfassemble in situ or on-site to kill both metastatic castrationresistant prostate cancer (mCRPC) and osteoblast cells in TMEs.

A prominent feature of osteoblastic mCRPC at the TME is that mCRPC and osteoblasts overexpress prostatic acid phosphatase (PAP)⁶ and alkaline phosphatase (ALP),⁷ respectively. However, developing inhibitors of PAP and ALP to treat mCRPC has been unsuccessful for several reasons: (i) PAP acts as a tumor suppressor,⁸ (ii) inhibitors of ALP are unable to inhibit cancer cells,⁹ and (iii) most phosphatases previously are considered as undruggable targets.^{10,11} Thus, we decided to explore EISA, which kills cancer cells by enzymatic reaction and self-assembly,¹² for developing therapeutics for osteoblastic mCRPC. EISA is particularly attractive because

EISA kills cancer cells without inhibiting the targeted enzymes. Moreover, ALP is metabolically inert in serum, ¹³ a subtlety allowing EISA to occur at TMEs. Recently, a variety of small molecule substrates, including peptides, ^{14–18} carbohydrates, ¹⁹ and lipids, ^{20,21} of ALP-based EISA are able to induce death of the cancer cells that overexpress ALP because EISA allows "onsite" generation of nanostructures from small molecules. ²² Although peptide-based substrates are the most explored among these building blocks up-to-date, their efficacy for killing mCRPC still remains to be improved. ²³ Thus, we choose to examine other nonpeptidic molecules as the self-assembling building blocks for EISA against mCRPC.

On the basis of aggregate advisors²⁴ and rigid-rod molecules for self-assembly, we choose a rigid-rod aromatic molecule, biphenyl, as the core motif for developing EISA substrates of PAP and ALP. Biphenyl has found various applications in liquid crystals, ^{25–28} dendrimers, ²⁹ long-range self-assembly, ³⁰ amphiphiles, ³¹ and peptides. ³² We recently found that biphenyl enables rapid enzymatic self-assembly and hydrogelation of peptides. ³³ But biphenyl has yet to be explored for EISA without involving peptides. On the basis of the above rationale, we phosphorylated the hydroxyl and conjugated a fluorophore (nitrobenzoxadiazole (NBD)) at the carboxylic end of hydroxybiphenylcarboxylate (BP) or hydroxyterphenylcarboxylate (TP) to produce pBP-NBD (1P) or pTP-NBD (2P), respectively. As a substrate of both PAP and ALP, 1P effectively

Received: May 24, 2022 Published: July 18, 2022

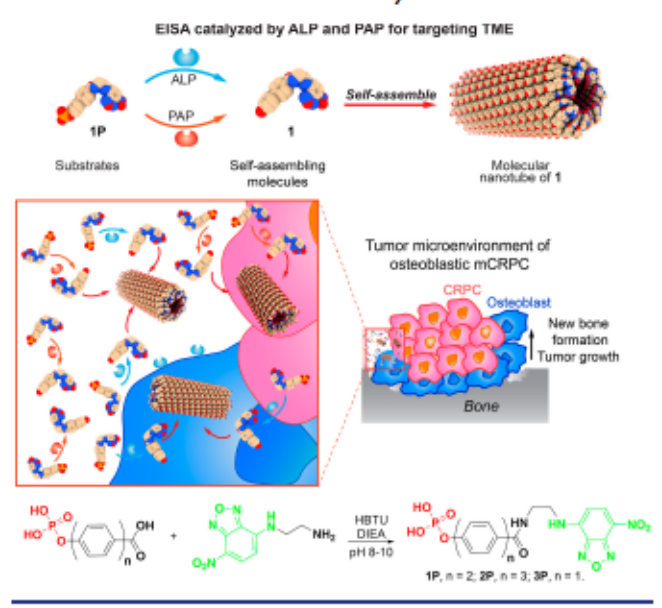




kills both metastatic castration-resistant prostate cancer cells (mCRPCs) (VCaP or PC3) and osteoblast mimic cells (Saos2) in their coculture. Fluorescent imaging shows that 1P enters Saos2 almost instantly to target the endoplasmic reticulum (ER) of the cells and that Saos2 in the coculture boosts the cellular uptake of 1P or 2P by VCaP or PC3 cells. Cryo-EM reveals that the 1 (from dephosphorylating 1P at physiological pH) or 1P (at acidic pH) self-assembles to form cones with C7 symmetry, and the supramolecular cones stack helically with a 3.5 Å rise to form nanotubes. Besides reporting the atomistic structure of nanotubes formed by the assembly of rigid-rod aromatics, this work, using enzymatic reactions to form intracellular nanotubes of small rigid-rod molecules, expands the pool of molecules for designing EISA substrates that selectively target TME.

Scheme 1 shows the structures and the key synthetic steps for making, 1P, 2P, and 3P, which have biphenyl, terphenyl, and

Scheme 1. EISA for Simultaneously Killing mCRPC and Osteoblast Cells and the Relevant Synthesis



phenyl motifs, respectively. While BP and hydroxylphenylcarboxylate are commercially available, TP is produced in almost quantitative yield from 4-bromo-4'-hydroxylbiphenyl and 4carboxyphenylboronic acid by palladium-catalyzed cross coupling.³⁴ Mixing BP or hydroxylphenylcarboxylate with phosphorus pentachloride directly under heat or reacting TP with phosphorus oxychloride in pyridine produces the phosphorylated aromatic carboxylic acids. After getting all three phosphorylated compounds, we conjugated them with NBDethylenediamine to generate 1P, 2P, and 3P.

As shown by transmission electron microscopy (TEM), adding ALP to a solution of 1P ($500 \,\mu\text{M}$ and pH 7.4) transforms the amorphous aggregates of 1P to ~ 7 nm diameter nanotubes of 1 (Figure 1). At pH 5.6, 1P ($50 \,\mu\text{M}$) forms nanotubes like those of 1. These results indicate 1P self-assembles more readily at lower pH because protonation decreases phosphate repulsion. Adding PAP in the 1P solution ($50 \,\mu\text{M}$ and at pH 5.6) results in more nanotubes (Figure 1). Adding ALP to the solution of 2P also switches the aggregates of 2P into nanotubes with similar diameters (Figure S2). At pH 5.6, 2P ($50 \,\mu\text{M}$) transforms from aggregates into twisted nanoribbons (Figure S1). 3P exists as amorphous aggregates both at pH 7.4 or pH 5.6 and rarely forms nanotubes after adding ALP or PAP (Figure S1), indicating that

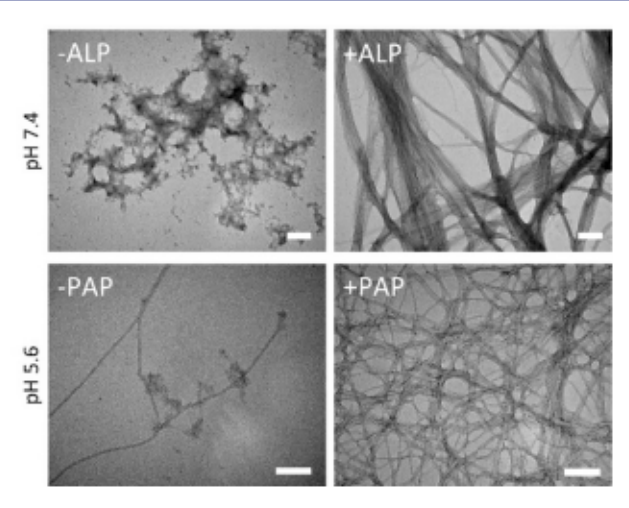


Figure 1. TEM of 1P ($500 \mu M$, pH 7.4) before and after adding ALP (0.1 U/mL) for 24 h and of 1P ($50 \mu M$, pH 5.6) before and after adding PAP (0.1 U/mL) for 24 h. Scale bar: 100 nm.

noncovalent interactions from phenyl are insufficient for 3P or 3 to self-assemble into nanotubes.

We tested 1P for its activity against six different cell lines, Saos2, SJSA1, VCaP, PC3, HepG2, and PNT1A (Figures 2A and S4). 1P shows the first day IC_{50} around 20.9 μ M against Saos2 cells. The IC50 values of 1P against SJSA1 and Saos2 are comparable, except day 1. While 1P significantly inhibits VCaP and PC3 cells from day 2 and day 3, respectively, 1P is rather compatible with HepG2 and PNT1A even at day 3, with IC50 around 108 μ M and 89 μ M. Even though 2P showed potent activity against Saos2 and SJSA1, it hardly inhibits VCaP, PC3, HepG2, and PNT1A (Figures S3 and S4). Compared to 1P and 2P, 1 and 2 are more toxic to the normal prostate cells, PNT1A, indicating that phosphorylation enhances the selectivity for targeting cancer cells. ALP inhibitor (DQB) reduces the cytotoxicity of 1P and 2P against Saos2 or SJSA1 cells (Figure S5), indicating that ALP-catalyzed EISA of 1P and 2P contributes to their cytotoxicity. The low cytotoxicity of 1P and 2P toward hepatocytes (HepG2) indicates a low toxicity of 1P and 2P to the liver. 3P hardly inhibits these cells (Figure S2B), consistent with the poor self-assembling ability of 3. M-β-CD, an inhibitor for caveolae mediated endocytosis, rescues Saso2 and SJSA1 treated by 1P or 2P, suggesting that 1P or 2P enters the cells via endocytosis (Figure S6).

As shown in Figure 2B, 1P enters Saos2 or SJSA1 within 1 min and accumulates inside the cells. On the other hand, 1P accumulates in VCaP or PC3 cells slowly, so that visible fluorescence from 1 emerges in VCaP and PC3 cells after 30 and 60 min, respectively. The inhibitory activity of 1P correlates well with the rate of cellular uptake, except in the case of HepG2. Although 1P enters HepG2 faster (Figure S7) than entering PC3, 1P hardly inhibits HepG2, agreeing with the detoxification function of hepatocytes. The similar trend as that of 1P to enter Saos2, SJSA1, VCaP, and PC3 cells (Figure S9). Agreeing with its cell compatibility, 3P enters Saos2 much slower than 1P or 2P does (Figure S8).

For Saos2 and SJSA1 cells, the distribution of 1P in cytosol resembles that of ER (Figures 2C and S10). Co-staining 1P with ER-tracker, Lyso-tracker, or Mito-tracker in Saos2 or SJSA1 cells shows that the fluorescence from 1P mostly overlaps with the fluorescence of ER-tracker, indicating that 1P, after entering cells and being dephosphorylated, specifically localizes in ER of

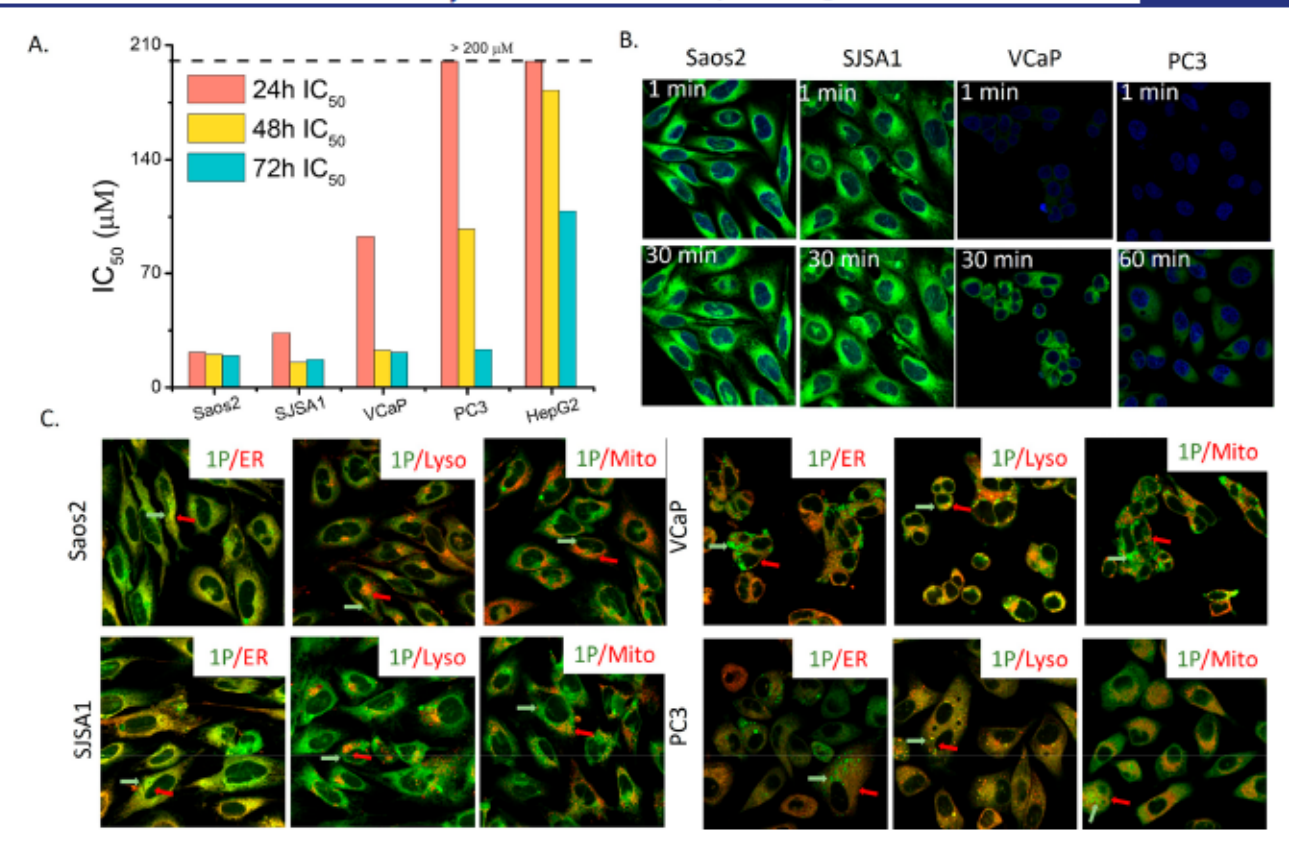


Figure 2. (A) IC_{50} of 1P incubated with Saos2, SJSA1, VCaP, PC3, and HepG2 cells. (B) Instant cell entry of 1P (100 μ M). (C) Intracellular distribution of 1P (50 μ M) in Saos2, SJSA1, VCaP, and PC3 after 4 h incubation. Red arrows indicate the marker, green arrow indicates 1. Yellow indicates their colocalization.

Saos2 and SJSA1. The ER accumulation agrees with that phosphobipenyl is a substrate of PTP1B, ³⁶ which mainly locates at ER. ³⁷ **2P** localizes more in ER of Saos2 and SJSA1 cells than in lysosomes and mitochondria, and forms denser fluorescent puncta in Saos2 and SJSA1 than **1P** does (Figures S11 and S12). The fluorescence of **1P** in VCaP and PC3 cells overlaps more with that of Lyso-tracker, indicating that **1P** mainly undergoes dephosphorylation in the lysosomes. This result agrees with that of PAP localized in lysosome. ³⁸

We cocultured the mCRPC cells (e.g., VCaP or PC3) and the osteoblast mimic cells (Saos2) in a 1:1 ratio to create a mimetic bone microenvironment and tested the efficacy of 1P. As shown in Figure 3A, after being incubated with 1P for 24 h, the viability of Saos2 or VCaP cells is 1.6% and 41.3%, respectively. The cell viability of the coculture of Saos2 and VCaP is 1.9% after adding 1P in the coculture. Similarly, 2P inhibits VCaP more effectively in the coculture. Moreover, Figure 3B shows the viability of PC3 cells, after being incubated with 1P or 2P in the coculture of PC3 and Saos2, is significantly lower than that of PC3 cells alone. These results suggest that Saos2 in the coculture significantly enhances the inhibitory activity of 1P or 2P against VCaP or PC3 cells. Fluorescence imaging reveals the cellular uptake of 1P by VCaP or PC3 cells (Figures 3C,D, S13-S15). The fluorescence in the VCaP or PC3 cells increases faster in the coculture than being cultured alone. These results indicate that Saos2 cells, in the coculture, boost the cellular uptake of 1P or 2P by VCaP and PC3 cells, thus leading to more effective inhibition of VCaP or PC3 cells.

We used cryo-EM and determined the high-resolution nanotube structures of both 1 at pH 7.4 and 1P at pH 5.6 (Figures S16A and S17A). Possible helical symmetries were

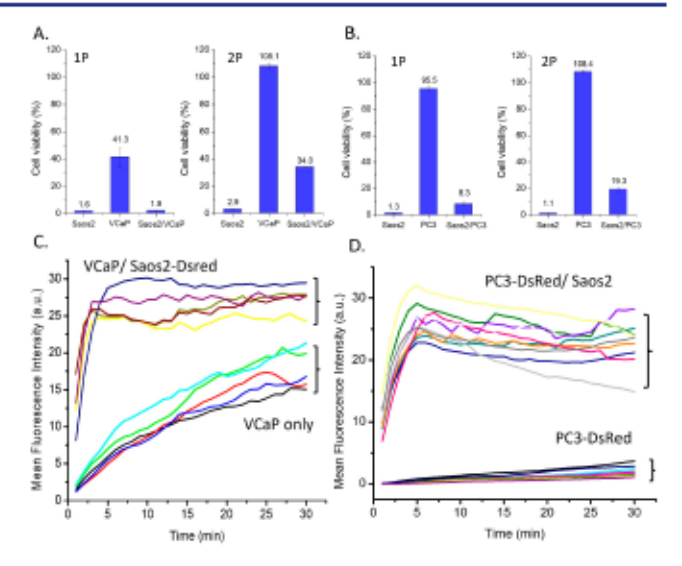


Figure 3. Viabilities of cells treated by 1P (100 μ M) or 2P (50 μ M) in (A) Saos2, VCaP, and the coculture of Saos2 and VCaP and in (B) Saos2, PC3, and the coculture of Saos2 and PC3. The mean fluorescence intensities of 1P (50 μ M) in (C) VCaP and the VCaP cocultured with Saos2-DsRed and (D) PC3-DsRed cells and the PC3-DsRed cocultured with Saos2 (each line representing one cell).

calculated from the averaged power spectrum of boxed filaments (Figures S16B and S17B) and the correct ones were found.³⁹ The nanotubes of 1 and 1P have almost identical diameters (Figure 4A,B) and helical symmetries (Figure 4C,D, Table S1), with aromatic rings held together by extensive pi-stacking interactions (Figure 4E). The NBD motifs point to the center

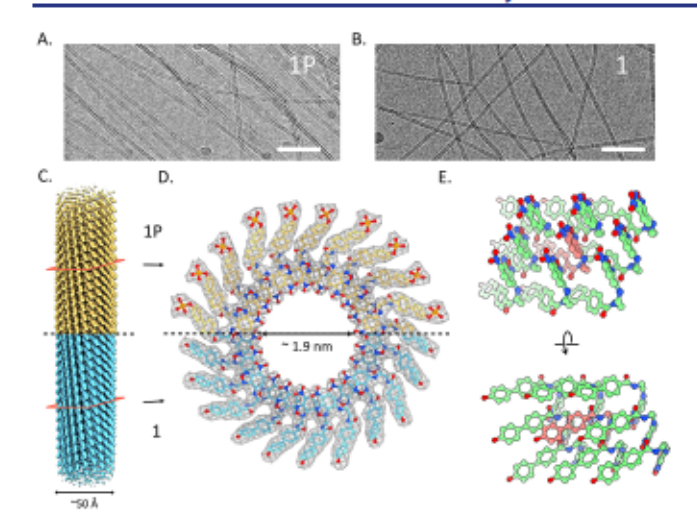


Figure 4. Cryo-EM images of the filaments of (A) 1P and (B) 1. Scale bar 50 nm. (C) 3D reconstruction of tubes of 1P and 1 from cryo-EM. (D) Top view of tubes of 1P and 1; phosphate of 1P can be seen at the periphery. (E) Side view of tubes of 1.

and the biphenyl groups constitute the periphery of the nanotubes. The ability of 1P to form nanotubes at pH 5.6 is consistent with the lysosomal accumulation of 1P (Figure 2A,C) and its increased activities against VCaP and PC3 cells after 48 h.

In summary, this work reports a new class of EISA substrates to form nanotubes for effectively killing osteoblast model cells and mCRPCs in a mimetic bone TME. The toxicity of 1 and 2 to PNT1A implies that nanotubes of 1 or 2 likely result in cell death. It illustrates the dual targeting mode-of-action of EISA substrates, which promise to kill both cancer and osteoblast cells at bone TMEs. Although the detailed mechanism of action of EISA of 1P or 2P in the coculture remains to be elucidated, using the enzymatic feature of TMEs to boost cellular uptake of EISA substrates in mCRPCs promises a new way to target TMEs of mCRPCs. The approach reported here should be applicable to other aggregation-prone small molecules or drug candidates, ^{24,40} which may lead to more effective EISA substrates for targeting TMEs of other metastatic cancers.

ASSOCIATED CONTENT

Supporting Information

The Supporting Information is available free of charge at https://pubs.acs.org/doi/10.1021/jacs.2c05491.

Materials and detailed experimental procedures, TEM and CLSM images, cell viabilities, chemical structures of the compounds (PDF)

Coordinates of the cryo-EM structures (PDB)

Coordinates of the cryo-EM structures (PDB)

AUTHOR INFORMATION

Corresponding Authors

Jer-Tsong Hsieh – Department of Urology, Southwestern Medical Center, University of Texas, Dallas, Texas 75235, United States; Email: jt.hsieh@utsouthwestern.edu

Edward H. Egelman — Department of Biochemistry and Molecular Genetics, University of Virginia, Charlottesville, Virginia 22908, United States; o orcid.org/0000-0003-4844-5212; Email: egelman@virginia.edu Bing Xu — Department of Chemistry, Brandeis University, Waltham, Massachusetts 02453, United States; ⊙ orcid.org/ 0000-0002-4639-387X; Email: bxu@brandeis.edu

Authors

Meihui Yi — Department of Chemistry, Brandeis University, Waltham, Massachusetts 02453, United States; orcid.org/ 0000-0002-1912-1043

Fengbin Wang — Department of Biochemistry and Molecular Genetics, University of Virginia, Charlottesville, Virginia 22908, United States; o orcid.org/0000-0003-1008-663X

Weiyi Tan — Department of Chemistry, Brandeis University, Waltham, Massachusetts 02453, United States; orcid.org/ 0000-0001-5316-8278

Complete contact information is available at: https://pubs.acs.org/10.1021/jacs.2c05491

Notes

The authors declare no competing financial interest.

ACKNOWLEDGMENTS

This work is partially supported by NIH CA142746 (B.X.) and CA252364 (B.X. and J.-T.H.), GM122510 (E.H.E.), K99GM138756 (F.W.), and NSF DMR-2011846 (B.X.).

REFERENCES

- (1) Cancer Facts & Figures 2022; American Cancer Society: Atlanta, 2022.
- (2) Pego, E. R.; Fernández, I.; Núñez, M. J. Molecular basis of the effect of MMP-9 on the prostate bone metastasis: A review. Urol. Oncol. Semin. Orig. Invest. 2018, 36 (6), 272–282.
- (3) Zhang, W.; Bado, I. L.; Hu, J.; Wan, Y. W.; Wu, L.; Wang, H.; Gao, Y.; Jeong, H. H.; Xu, Z.; Hao, X.; Lege, B. M.; Al-Ouran, R.; Li, L.; Li, J.; Yu, L.; Singh, S.; Lo, H. C.; Niu, M.; Liu, J.; Jiang, W.; Li, Y.; Wong, S. T. C.; Cheng, C.; Liu, Z.; Zhang, X. H. The bone microenvironment invigorates metastatic seeds for further dissemination. Cell 2021, 184 (9), 2471–2486.
- (4) Cha, T. L.; Wu, T. T. L.; Vogelzang, N. J.; Huang, C. Y.; Huang, S. P.; Lin, C. C.; Ou, Y. C.; Pang, S. T.; Shen, D. H. Y.; Wu, W. J.; Chang, W. Y. H. Optimal usage of radium-223 in metastatic castration-resistant prostate cancer. J. Formos. Med. Assoc. 2017, 116 (11), 825–836.
- (5) Suominen, M. I.; Fagerlund, K. M.; Rissanen, J. P.; Konkol, Y. M.; Morko, J. P.; Peng, Z.; Alhoniemi, E. J.; Laine, S. K.; Corey, E.; Mumberg, D.; Ziegelbauer, K.; Käkönen, S. M.; Halleen, J. M.; Vessella, R. L.; Scholz, A. Radium-223 inhibits osseous prostate cancer growth by dual targeting of cancer cells and bone microenvironment in mouse models. Clin. Cancer Res. 2017, 23 (15), 4335–4346.
- (6) Kirschenbaum, A.; Liu, X. H.; Yao, S.; Leiter, A.; Levine, A. C. Prostatic acid phosphatase is expressed in human prostate cancer bone metastases and promotes osteoblast differentiation. In Ann. N.Y. Acad. Sci.; Blackwell Publishing Inc., 2011; Vol. 1237, pp 64—70.
- (7) Heinrich, D.; Bruland, O.; Guise, T. A.; Suzuki, H.; Sartor, O. Alkaline phosphatase in metastatic castration-resistant prostate cancer: Reassessment of an older biomarker. Future Oncology 2018, 14 (24), 2543–2556.
- (8) Lin, M.-F.; Lee, M.-S.; Zhou, X.-W.; Andressen, J. C.; Meng, T.-C.; Johansson, S. L.; West, W. W.; Taylor, R. J.; Anderson, J. R.; Lin, F.-F. Decreased Expression of Cellular Prostatic Acid Phosphatase Increases Tumorigenicity of Human Prostate Cancer Cells. J. Urol. 2001, 166 (5), 1943–1950.
- (9) Wang, H.; Feng, Z.; Wang, Y.; Zhou, R.; Yang, Z.; Xu, B. Integrating Enzymatic Self-Assembly and Mitochondria Targeting for Selectively Killing Cancer Cells without Acquired Drug Resistance. J. Am. Chem. Soc. 2016, 138 (49), 16046–16055.
- (10) Stanford, S. M.; Bottini, N. Targeting Tyrosine Phosphatases: Time to End the Stigma. Trends Pharmacol. Sci. 2017, 38 (6), 524-540.

- (11) Vainonen, J. P.; Momeny, M.; Westermarck, J. Druggable cancer phosphatases. Sci. Trans. Med. 2021, 13 (588), No. eabe2967.
- (12) He, H.; Tan, W.; Guo, J.; Yi, M.; Shy, A. N.; Xu, B. Enzymatic Noncovalent Synthesis. Chem. Rev. 2020, 120 (18), 9994–10078.
- (13) Kaplan, M. M. Alkaline phosphatase. N Engl J. Med. 1972, 286 (4), 200-2.
- (14) Yang, Z. M.; Xu, K. M.; Guo, Z. F.; Guo, Z. H.; Xu, B. Intracellular Enzymatic Formation of Nanofibers Results in Hydrogelation and Regulated Cell Death. Adv. Mater. 2007, 19 (20), 3152–3156.
- (15) Kuang, Y.; Shi, J.; Li, J.; Yuan, D.; Alberti, K. A.; Xu, Q.; Xu, B. Pericellular hydrogel/nanonets inhibit cancer cells. Angew. Chem., Int. Ed. Engl. 2014, 53 (31), 8104-7.
- (16) Tanaka, A.; Fukuoka, Y.; Morimoto, Y.; Honjo, T.; Koda, D.; Goto, M.; Maruyama, T. Cancer cell death induced by the intracellular self-assembly of an enzyme-responsive supramolecular gelator. J. Am. Chem. Soc. 2015, 137 (2), 770-5.
- (17) Zhou, J.; Du, X.; Yamagata, N.; Xu, B. Enzyme-Instructed Self-Assembly of Small D-Peptides as a Multiple-Step Process for Selectively Killing Cancer Cells. J. Am. Chem. Soc. 2016, 138 (11), 3813–23.
- (18) Gao, Y.; Kuang, Y.; Guo, Z. F.; Guo, Z.; Krauss, I. J.; Xu, B. Enzyme-instructed molecular self-assembly confers nanofibers and a supramolecular hydrogel of taxol derivative. J. Am. Chem. Soc. 2009, 131 (38), 13576-7.
- (19) Pires, R. A.; Abul-Haija, Y. M.; Costa, D. S.; Novoa-Carballal, R.; Reis, R. L.; Ulijn, R. V.; Pashkuleva, I. Controlling cancer cell fate using localized biocatalytic self-assembly of an aromatic carbohydrate amphiphile. J. Am. Chem. Soc. 2015, 137 (2), 576—9.
- (20) Wang, H.; Feng, Z.; Wu, D.; Fritzsching, K. J.; Rigney, M.; Zhou, J.; Jiang, Y.; Schmidt-Rohr, K.; Xu, B. Enzyme-Regulated Supramolecular Assemblies of Cholesterol Conjugates against Drug-Resistant Ovarian Cancer Cells. J. Am. Chem. Soc. 2016, 138 (34), 10758-61.
- (21) Wang, J.; Tan, W.; Li, G.; Wu, D.; He, H.; Xu, J.; Yi, M.; Zhang, Y.; Aghvami, S. A.; Fraden, S.; Xu, B. Enzymatic Insertion of Lipids Increases Membrane Tension for Inhibiting Drug Resistant Cancer Cells. Chemistry 2020, 26 (66), 15116–15120.
- (22) Parak, W. J.; Weil, T.; Weiss, P. S. A Virtual Issue on Nanomedicine. ACS Nano 2021, 15 (10), 15397-15401.
- (23) Feng, Z.; Wang, H.; Yi, M.; Lo, C. Y.; Sallee, A.; Hsieh, J. T.; Xu, B. Instructed-Assembly of Small Peptides Inhibits Drug-Resistant Prostate Cancer Cells. Pept. Sci. 2020, 112 (1), No. e24123.
- (24) Irwin, J. J.; Duan, D.; Torosyan, H.; Doak, A. K.; Ziebart, K. T.; Sterling, T.; Tumanian, G.; Shoichet, B. K. An Aggregation Advisor for Ligand Discovery. J. Med. Chem. 2015, 58 (17), 7076–87.
- (25) Durbin, S. D.; Arakelian, S. M.; Shen, Y. R. Optical-field-induced birefringence and Freedericksz transition in a nematic liquid crystal. *Phys. Rev. Lett.* **1981**, *47* (19), 1411–1414.
- (26) Kouwer, P. H. J.; Swager, T. M. Synthesis and mesomorphic properties of rigid-core ionic liquid crystals. J. Am. Chem. Soc. 2007, 129 (45), 14042–14052.
- (27) Kato, T.; Hirota, N.; Fujishima, A.; Fréchet, J. M. J. Supramolecular hydrogen-bonded liquid-crystalline polymer complexes. Design of side-chain polymers and a host-guest system by noncovalent interaction. J. Polym. Sci. Part A 1996, 34 (1), 57–62.
- (28) Cao, Y.; Alaasar, M.; Zhang, L.; Zhu, C.; Tschierske, C.; Liu, F. Supramolecular meso-Trick: Ambidextrous Mirror Symmetry Breaking in a Liquid Crystalline Network with Tetragonal Symmetry. J. Am. Chem. Soc. 2022, 144 (15), 6936–6945.
- (29) Peterca, M.; Imam, M. R.; Leowanawat, P.; Rosen, B. M.; Wilson, D. A.; Wilson, C. J.; Zeng, X.; Ungar, G.; Heiney, P. A.; Percec, V. Self-assembly of hybrid dendrons into doubly segregated supramolecular polyhedral columns and vesicles. J. Am. Chem. Soc. 2010, 132 (32), 11288–11305.
- (30) Van Esch, J.; De Feyter, S.; Kellogg, R. M.; De Schryver, F.; Feringa, B. L. Self-assembly of bisurea compounds in organic solvents and on solid substrates. Chem. Eur. J. 1997, 3 (8), 1238–1243.
- (31) Kunitake, T.; Okahata, Y.; Shimomura, M.; Yasunami, S. I.; Takarabe, K. Formation of Stable Bilayer Assemblies in Water from Single-Chain Amphiphiles. Relationship between the Amphiphile

- Structure and the Aggregate Morphology. J. Am. Chem. Soc. 1981, 103 (18), 5401-5413.
- (32) Nesloney, C. L.; Kelly, J. W. A 2,3'-substituted biphenyl-based amino acid facilitates the formation of a monomeric β -hairpin-like structure in aqueous solution at elevated temperature. *J. Am. Chem. Soc.* 1996, 118 (25), 5836–5845.
- (33) Yi, M.; Guo, J.; He, H.; Tan, W.; Harmon, N.; Ghebreyessus, K.; Xu, B. Phosphobisaromatic motifs enable rapid enzymatic self-assembly and hydrogelation of short peptides. Soft Matter 2021, 17, 8590–8594.
- (34) Jansa, J.; Reznícek, T.; Jambor, R.; Bureš, F.; Lycka, A. Synthesis of Hydroxy-Substituted p-Terphenyls and some Larger Oligophenylenes via Palladium on Charcoal Catalyzed Suzuki-Miyaura Reaction. Advanced Synthesis & Catalysis 2017, 359 (2), 339–350.
- (35) Miners, J. O.; Knights, K. M.; Houston, J. B.; Mackenzie, P. I. In vitro—in vivo correlation for drugs and other compounds eliminated by glucuronidation in humans: Pitfalls and promises. *Biochem. Pharmacol.* 2006, 71 (11), 1531–1539.
- (36) Montserat, J.; Chen, L.; Lawrence, D. S.; Zhang, Z. Y. Potent low molecular weight substrates for protein-tyrosine phosphatase. *J. Biol. Chem.* 1996, 271 (13), 7868–7872.
- (37) Haj, F. G.; Verveer, P. J.; Squire, A.; Neel, B. G.; Bastiaens, P. I. H. Imaging Sites of Receptor Dephosphorylation by PTP1B on the Surface of the Endoplasmic Reticulum. *Science* **2002**, 295 (5560), 1708–1711.
- (38) Tappel, A. Lysosomal and prostasomal hydrolytic enzymes and redox processes and initiation of prostate cancer. *Med. Hypotheses* **2005**, 64 (6), 1170–1172.
- (39) Wang, F.; Gnewou, O.; Solemanifar, A.; Conticello, V. P.; Egelman, E. H. Cryo-EM of Helical Polymers. *Chem. Rev.* 2022, DOI: 10.1021/acs.chemrev.1c00753.
- (40) McGovern, S. L.; Caselli, E.; Grigorieff, N.; Shoichet, B. K. A common mechanism underlying promiscuous inhibitors from virtual and high-throughput screening. J. Med. Chem. 2002, 45 (8), 1712–22.

Recommended by ACS

Triphosphate Prodrugs of the Anti-HIV-Active Compound 3'-Deoxy-3'-fluorothymidine (FLT)

Simon Weising, Chris Meier, et al.

SEPTEMBER 13, 2022

JOURNAL OF MEDICINAL CHEMISTRY

READ ☑*

Discovery of SHR2415, a Novel Pyrrole-Fused Urea Scaffold ERK1/2 Inhibitor

Xin Li, Weikang Tao, et al.

APRIL 01, 2022

ACS MEDICINAL CHEMISTRY LETTERS

READ (3

CRCM5484: A BET-BDII Selective Compound with Differential Anti-leukemic Drug Modulation

Kendall Carrasco, Stéphane Betzi, et al.

MARCH 29, 2022

JOURNAL OF MEDICINAL CHEMISTRY

READ ☑

Inhibitors of the Hippo Pathway Kinases STK3/MST2 and STK4/MST1 Have Utility for the Treatment of Acute Myeloid Leukemia

Nicole Bata, Nicholas D. P. Cosford, et al.

NOVEMBER 22, 2021

JOURNAL OF MEDICINAL CHEMISTRY

READ 🗹

Get More Suggestions >